

# Generating Event Triggers Based on Hilbert-Huang Transform and Its Application to Gravitational-Wave Data

Edwin J. Son<sup>1</sup>, Whansun Kim<sup>1</sup>, Young-Min Kim<sup>2</sup>, Jessica McIver<sup>3</sup>, John J. Oh<sup>1</sup> and Sang Hoon Oh<sup>1</sup>

<sup>1</sup> Division of Basic Researches for Industrial Mathematics, National Institute for Mathematical Sciences, Daejeon 34047, Republic of Korea

<sup>2</sup> School of Natural Science, Ulsan National Institute of Science and Technology, Ulsan 44919, Republic of Korea

<sup>3</sup> LIGO, California Institute of Technology, Pasadena, CA 91125, USA

E-mail: eddy@nims.re.kr, iou78@nims.re.kr, ymkim715@unist.ac.kr, jlmciver@caltech.edu, johnoh@nims.re.kr, shoh@nims.re.kr

2 April 2024

**Abstract.** We present a new event trigger generator based on the Hilbert-Huang transform, named EtaGen ( $\eta$ Gen). It decomposes a time-series data into several adaptive modes without imposing *a priori* bases on the data. The adaptive modes are used to find transients (excesses) in the background noises. A clustering algorithm is used to gather excesses corresponding to a single event and to reconstruct its waveform. The performance of EtaGen is evaluated by how many injections in the LIGO simulated data are found. EtaGen is viable as an event trigger generator when compared directly with the performance of Omicron, which is currently the best event trigger generator used in the LIGO Scientific Collaboration and Virgo Collaboration.

*Keywords:* Event trigger generator, Hilbert-Huang transform, GW data analysis

## 1. Introduction

Recently, the Laser Interferometer Gravitational-wave Observatory (LIGO) Scientific Collaboration (LSC) and Virgo collaboration announced the observations of confirmed gravitational-wave (GW) signals (GW150914, GW151226, GW170104, GW170608, GW170814, and GW170817) from the binary black hole mergers and a binary neutron star merger [1, 2, 3, 4, 5, 6]. In order to make these discoveries possible, the LSC-Virgo Collaboration (LVC) characterizes the data to mitigate a high rate of transient noise that can mimic or bias the source property estimation of true GW events [7, 8]. The event trigger generators are a critical tool for identifying and characterizing transient noise. Event trigger generators extract instances of excess power from a time series,

called *event triggers*. Most of the event trigger generators in the LVC impose wavelets as a basis set, which offer coarse time resolution at low frequencies [9].

Here, we introduce an adaptive time-series analysis method, the Hilbert-Huang transform (HHT) [10] to improve time resolution at low frequency, where there might be harmful noise sources such as earthquakes and light scattering as common problems that limit interferometer uptime and hinder the astrophysical searches. Moreover, in the third generation interferometer era like *Cosmic Explorer*, the low-frequency band noise will become crucial in the major detector sensitivity.

The HHT consists of the empirical mode decomposition (EMD) and the Hilbert spectral analysis. The EMD decomposes a time-series data into several adaptive modes<sup>‡</sup>, called intrinsic mode functions (IMFs), without imposing a basis set. Then, the Hilbert spectral analysis calculates the instantaneous amplitude and instantaneous frequency of each IMFs. It is a remarkable property of this adaptive approach that relieves the uncertainty principle in the signal processing [9]. The time resolution of each IMF is the same with that of the input data even in the low frequency band. In this respect and by virtue of its adaptive nature, the HHT has been extensively used in the various area such as biomedical application of Electroencephalography data, financial analysis, geophysical and meteorological data analysis, etc (for more references, see [11]). In particular, it has been introduced and studied for GW signal search and noise detection in [12, 13, 14, 15, 16, 17].

In this paper, we propose a new event trigger generator based on the HHT, named *EtaGen* ( $\eta$ Gen). The instantaneous amplitude of each IMF is used to mark the regions which excess a certain amplitude cut, and those regions are referred to as *excesses*. The excesses in all the IMFs are characterized by their time and frequency informations, using the instantaneous frequency of the IMF. The event triggers are then obtained by clustering nearby excesses in time-frequency plane. Generated event triggers are used to diagnose correlations between transients in the GW data and the detectors' behavior and environment, as well as to characterize transient noise that impacts the astrophysical searches. One of byproduct of EtaGen is to reconstruct the original waveform by simply adding the time-series corresponding to the excesses clustered in each event trigger.

This paper is organized as follows. We first briefly review the HHT and introduce an online EMD method in section 2. Then, we describe the signal extraction and clustering algorithms of the EtaGen followed by waveform reconstruction method in section 3. Then the performance of EtaGen is found in section 4. Finally, conclusion and discussion are given in section 5.

<sup>‡</sup> Here we describe a mode to be adaptive if it is determined during the decomposition process that depends on the original time series data as oppose to the mode that are determined by the predefined basis set.

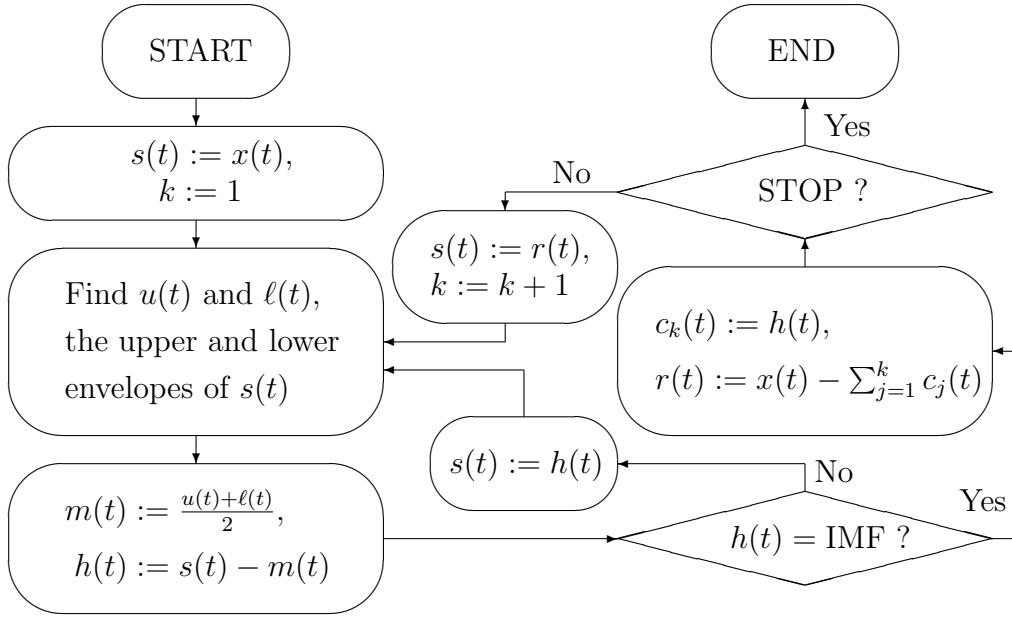


**Figure 1.** The flowchart of empirical mode decomposition (EMD). EMD does not use wavelets as a basis set. A segment of time-series data undergoes a process called *sifting*: the segment is subtracted by the mean of its envelopes to get an IMF (Step ii and iii of EMD). The remainder becomes an IMF if it satisfies a IMF criterion. Or the remainder undergoes sifting repeatedly until satisfying the criterion (Step iv). Once an IMF is obtained, it is subtracted from the original segment (Step v) to obtain a residual. And the whole process is repeated on the residual until it meets the ending criterion (Step vi). Refer to the text for more detail.

## 2. Hilbert-Huang Transform and weighted sliding EMD

The HHT is an extension of the Hilbert transform by adding the EMD to the Hilbert spectral analysis. The Hilbert transform  $\mathcal{H}[\cdot]$  is a linear operator used to obtain the analytic representation  $\tilde{x}(t) = x(t) + i\mathcal{H}[x](t)$  of a real function  $x(t)$ ,

$$\mathcal{H}[x](t) = \frac{1}{\pi} \mathcal{P} \int_{-\infty}^{\infty} d\tau \frac{x(\tau)}{t - \tau}, \quad (1)$$

where  $\mathcal{P}$  represents the principal value. The Hilbert spectral analysis then finds the instantaneous amplitude  $a(t) = ||\tilde{x}(t)||$  and the instantaneous frequency  $f(t) = (2\pi)^{-1}(\text{d}/\text{d}t) \arg[\tilde{x}(t)]$  from the analytic representation. In general, it is easy that the instantaneous amplitude and instantaneous frequency using the Hilbert spectral analysis fail to represent the accurate amplitude and frequency of the original time series  $x(t)$ . For example, if the given function is shifted by a constant,  $x(t) \rightarrow x(t) + x_0$ , the analytic representation is also shifted by the same amount,  $\tilde{x}(t) \rightarrow \tilde{x}(t) + x_0$ , leading the contaminated instantaneous amplitude and instantaneous frequency. To resolve this contamination, the EMD is introduced to decompose the given function into several IMFs that are well-behaved for the Hilbert spectral analysis.

The EMD is an adaptive process to obtain the IMFs from a time-series data  $x(t)$ .

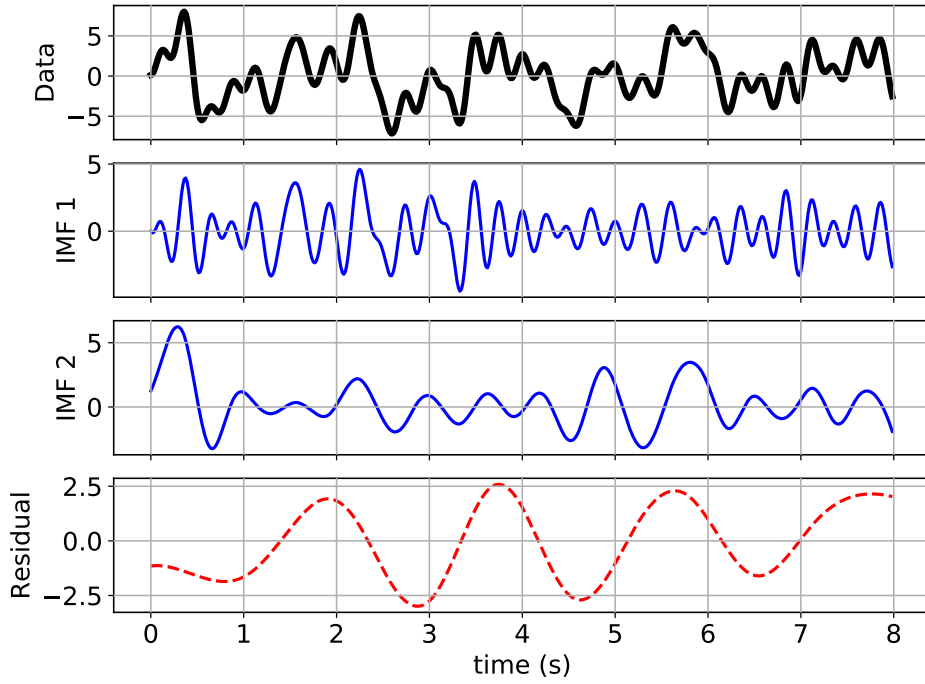


**Figure 2.** An example of EMD. The data (top, black, thick) is decomposed into the IMFs (middle, blue) and the residual (bottom, red, dashed). The first IMF is dominated by high frequency fluctuation, while the lower frequency features reside in the second IMF and the residual.

The algorithm of the EMD can be summarized as follows (see figure 1):

- (i) Set data to be sifted  $s(t) := x(t)$  and the IMF number  $k := 1$ .
- (ii) Find the upper and lower envelopes of  $s(t)$ , say  $u(t)$  and  $\ell(t)$ .
- (iii) Subtract the mean of the envelopes  $m(t) := \frac{1}{2}[u(t) + \ell(t)]$  from  $s(t)$  and set  $h(t) := s(t) - m(t)$ .
- (iv) If  $h(t)$  fails to satisfy a criterion for the IMF to be defined below, set  $s(t) := h(t)$  and go to step ii.
- (v) Otherwise, set  $k$ -th IMF  $c_k(t) := h(t)$  and the residual  $r(t) := x(t) - \sum_{j=1}^k c_j(t)$ .
- (vi) If  $r(t)$  fails to satisfy ending criterion for the EMD, set  $s(t) := r(t)$  and  $k := k + 1$  then go to step ii.
- (vii) Otherwise, finish the EMD with  $k$  IMFs  $c_j(t)$  and the residual  $r(t)$ .

In the literatures, the Cauchy type criterion [10], the mean value criterion [18], and the  $S$ -number criterion [19] are widely used for the step iv (for a review, see [20]). In the examples in this paper, the  $S$ -number criterion will be implicitly considered. The  $S$ -number criterion restricts the difference between the numbers of extrema and zero-crossings of an IMF. For the step vi, the criterion is given by the number of the IMFs or the number of extrema of the residual  $r(t)$ . An example of the EMD is shown in figure 2.

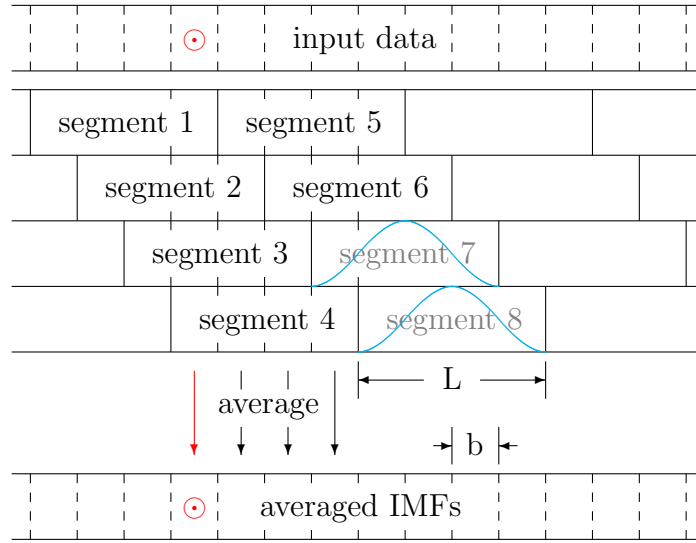


**Figure 3.** An example of weighted SEMD for  $N = 4$ . The length of each segment is  $L = Nb$ , where  $b$  is the length of a block. The segments  $n$  and  $(n + 1)$  are overlapped by the length of  $(N - 1)b$  and each block is shared by four segments. For example, the block marked with  $\odot$  is shared by segments 1, 2, 3 and 4. The EMD process decomposes each segment into the corresponding IMFs, which will then be multiplied by a weighting function. The weighting function is shown in segments 7 and 8. Then, the IMFs of all the segments in a shared block are averaged out with the weighting function. For the block  $\odot$ , the IMFs in the last block of the segment 1, in the second last of 2, in the second of 3 and in the first of 4 are weighted-averaged. When the weighting function is a nonzero constant function, the weighted SEMD reduces to the SEMD.

The EMD approach can be extended in a number of ways, some of which are important here so that they help to improve the accuracy of decomposition and to suppress the computation cost. The ensemble EMD is introduced in order to obtain more accurate IMFs [21]. It applies step ii of EMD to an ensemble of whitened data and their averaged value as a true result, which reduces the noise perturbation around the true solution and enhance the precision of IMFs. In general, however, it is inappropriate to use the ensemble EMD in an online data analysis because of its expensive computing cost. This drawback can be also resolved by the sliding EMD (SEMD) [22] and/or its extension, weighted SEMD [23]. The algorithm of SEMD is somewhat simple (see figure 3):

- (i) The input data is split into segments of length  $L$ , where each segment can be split into  $N$  blocks of length  $b = L/N$  and is overlapped with the next segment by  $(N - 1)$  blocks, that is, each block is shared by  $N$  segments.
- (ii) Each segment is decomposed by the EMD process.
- (iii) The IMFs of the segments are averaged out in each block.

The weighted SEMD introduces a *weighting function* on averaging process in step iii,

which reduces the edge effects at both sides of each segment originated from the EMD and from the SEMD as well. The authors in [23] suggest a Gaussian weighting function,  $w(n) = \exp\left\{\frac{1}{2}[2\alpha n/(L-1)]^2\right\}$  with  $\alpha = 2.5$  and  $-\frac{1}{2}(L-1) \leq n \leq \frac{1}{2}(L-1)$ . This function, however, does not vanish at the ends of a segment, i.e.  $n = \pm\frac{1}{2}(L-1)$ , and thus the edge effect from the SEMD remains and causes a step function-like behavior in the IMFs. To moderate this unwanted behavior, we, here, propose a sinusoidal weighting function,

$$w(n) = \sin^2\left(\frac{\pi n}{L-1}\right), \quad n = 0, \dots, (L-1), \quad (2)$$

which vanishes at the edges and thus produces well-behaved IMFs in each segment.

Once the data  $x(t)$  is decomposed into IMFs  $c_j(t)$ , the analytic representation of each IMF is calculated by the Hilbert transform (1) to obtain its instantaneous amplitude and instantaneous frequency, say  $a_j(t)$  and  $f_j(t)$ . Then, we can recover the original data  $x(t)$  in terms of the instantaneous amplitudes and the instantaneous frequencies of the IMFs,

$$x(t) = \Re\left\{\sum_j a_j(t) \exp\left[2\pi i \int^t f_j(\tau) d\tau\right]\right\} + r(t), \quad (3)$$

where  $\Re(z)$  represents the real part of  $z$ . The residual  $r(t)$  is negligible in the analysis, since it contains in general only the lower frequency data than the frequency band under consideration. Note that the representation (3) of the HHT is similar to the discrete Fourier transform  $x(t) = \Re\left[\sum_j a_j \exp(2\pi i f_j t)\right]$  but the  $a_j(t)$  and the  $f_j(t)$  are not constant, which explains why the HHT has much smaller number of modes than the discrete Fourier transform because of the adaptive nature of the transform.

### 3. Event trigger generation algorithm of EtaGen

#### 3.1. EtaGen Algorithm I: Finding Excesses

We assume that the given data  $x(t) = n(t) + g(t)$  is whitened, in order to make the event trigger generation algorithm more or less simple. Here we define  $x(t)$  as the data,  $n(t)$  as the background noise, and  $g(t)$  as transients. Then, let  $\sigma$  be the standard deviation (STD) of the background noise, which definitely follows the Gaussian distribution. Since the data  $x(t)$  contains both the background noise and the transients, it is hard to estimate  $\sigma$ . We thus assume that the STD of the background Gaussian noise is proportional to the median absolute deviation (MAD) of  $x(t)$ ,

$$\sigma = \gamma \text{MAD}[x(t)], \quad (4)$$

where the coefficient  $\gamma$  is chosen to be 1.48 due to the fact that the ratio between the STD and the MAD of a Gaussian noise is given by  $\left[\sqrt{2} \text{erf}^{-1}\left(\frac{1}{2}\right)\right]^{-1} \approx 1.48$ . Note that  $x(t)$  contains transients in general and its MAD is thus larger than the MAD of the background Gaussian noise; furthermore, the STD and the MAD of a sine wave data

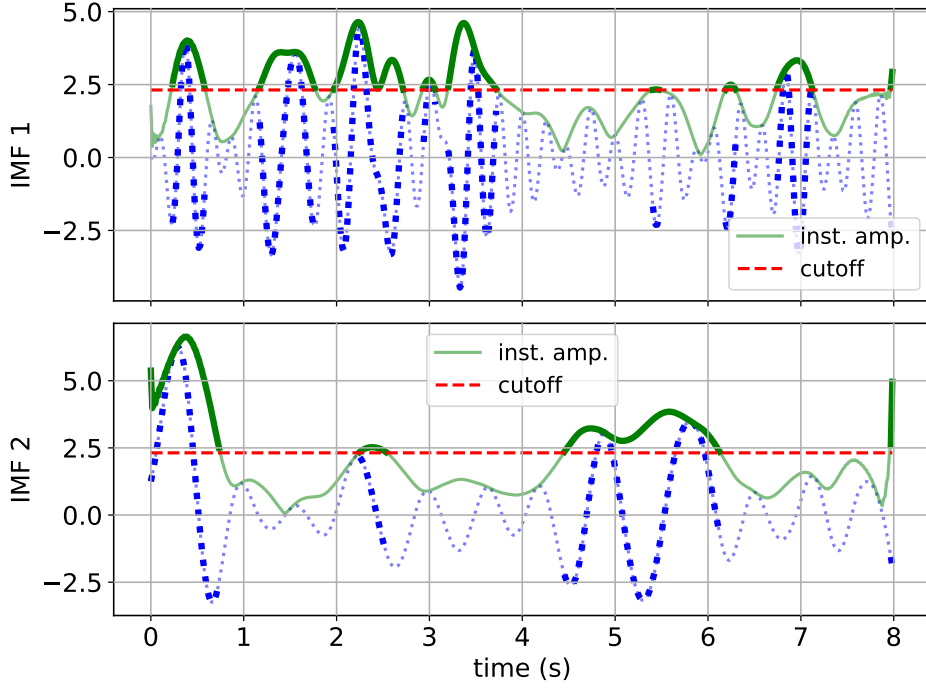


**Figure 4.** This plots show how to find excesses in the EtaGen. First, series of maxima in the instantaneous amplitude (thick green solid line) are identified in every IMF by putting cutoffs (red dashed line) in amplitude. The excesses are the segments of time series in IMFs corresponding to the series of maxima identified in the IMFs (thick blue dotted line). The information of an excess such as the peak amplitude, the peak time, the central frequency, the starting and end times and SNR is recorded if the SNR of the excess computed by (5) exceeds a given threshold,  $T$ . Refer to the text for more details.

are the same. However, if the Gaussian noise is dominant in the data  $x(t)$ , then the contributions of the transients to the MAD are negligible.

To find excesses, we introduce  $A_j$ , a set of maxima of the instantaneous amplitude  $a_j(t)$  of the  $j$ -th IMF  $c_j(t)$ . Then, setting a signal-to-noise ratio (SNR) threshold  $T$ , the excess finding algorithm for the  $j$ -th IMF is as follows:

- (i) Set a cutoff  $\sigma_j := \min\{\sigma, \text{MAD}[c_j(t)]\}$  and  $k := 1$ .
- (ii) Take  $k$ -th maximum  $A_{j,k}$  of the  $j$ -th instantaneous amplitude  $a_j(t)$ .
- (iii) If  $A_{j,k} < \sigma_j$ , then set  $k := k + 1$  and go to step ii. An example of maxima over the cutoff is depicted in figure 4.
- (iv) Otherwise, find the start and end times of the excess, say  $t_s$  and  $t_e$ , where we omit the indices  $j$  and  $k$  for convenience.
- (v) Calculate the SNR  $\rho$  of the excess.
- (vi) If  $\rho \geq T$ , then store the excess informations, such as the peak amplitude  $A_{j,k}$ , the peak time  $t_p$  where  $A_{j,k}$  is located, the peak frequency  $f_j(t_p)$ , the central time  $t_c = \mathcal{N} \int_{t_s}^{t_e} t a_j(t) dt$ , the central frequency  $f_c = \mathcal{N} \int_{t_s}^{t_e} f_j(t) a_j(t) dt$ , etc. as well as

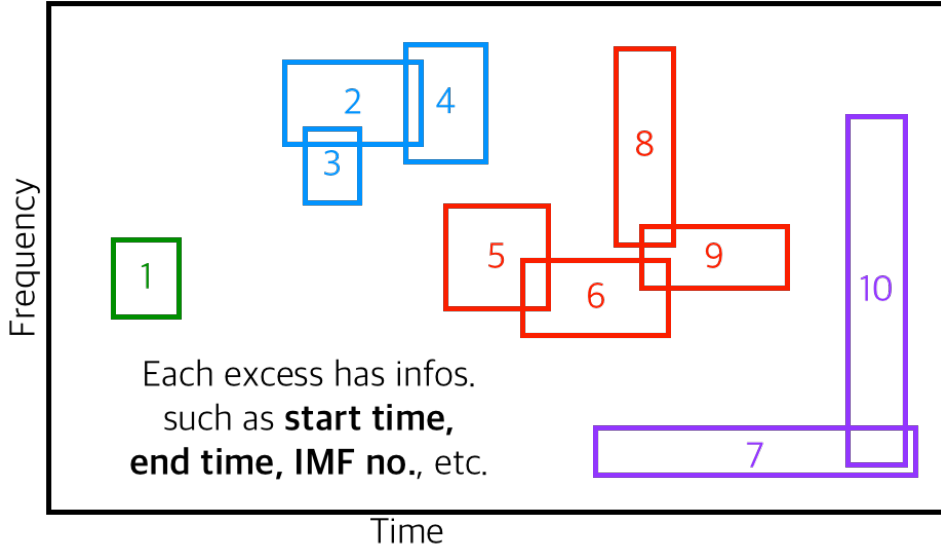


**Figure 5.** Illustration of clustering excesses. Each rectangle represents an excess in the time-frequency plane. It is defined by the starting and end time ( $t_s$  and  $t_e$ , respectively) and the low and high frequency ( $f_{\text{low}}$  and  $f_{\text{high}}$ , respectively) of the excess. Two or more rectangles are clustered in to a single event trigger if they overlap. For example, red rectangles are clustered into a single event trigger. And so are the light blue and purple ones.

$t_s$ ,  $t_e$ , and  $\rho$ , where  $\mathcal{N} = \left[ \int_{t_s}^{t_e} a_j(t) dt \right]^{-1}$ .

- (vii) If  $k$  is less than the number of the maxima  $A_j$ , then set  $k := k + 1$  and go to step ii.
- (viii) Otherwise, finish finding excesses for the  $j$ -th IMF and move on to the next IMF if exists.

To find  $t_s$  and  $t_e$  in the step iv, one might consider the use of the instantaneous amplitude: the times, when the nearest minima of  $a_j(t)$  to the peak amplitude  $A_{j,k}$  are located, can be set to  $t_s$  and  $t_e$ . However, the instantaneous amplitude is sometimes obtained as a sawtooth shape instead of the smooth bell shape for an excess. To resolve it, we introduce the extremum  $c_j^{(\text{ext})}$  of the  $j$ -th IMF  $c_j(t)$ , find the nearest minima of  $|c_j^{(\text{ext})}|$  to the peak amplitude  $A_{j,k}$ , and set  $t_s$  and  $t_e$  times when they are located. We then calculate the SNR of the excess corresponding to the peak amplitude  $A_{j,k}$  in the  $j$ -th IMF as

$$\rho_{j,k} = \frac{1}{\sigma} \left[ \int_{t_s}^{t_e} |c_j(t)|^2 dt \right]^{1/2}, \quad (5)$$

which agrees with the SNR definition shown in [13].

### 3.2. EtaGen Algorithm II: Clustering

A transient event signal as well as background noises should be split into several modes of IMF, which generates a set of excesses. We now gather such excesses together to get *an event trigger*. Among the parameters of each excess, the start time  $t_s$ , the end time



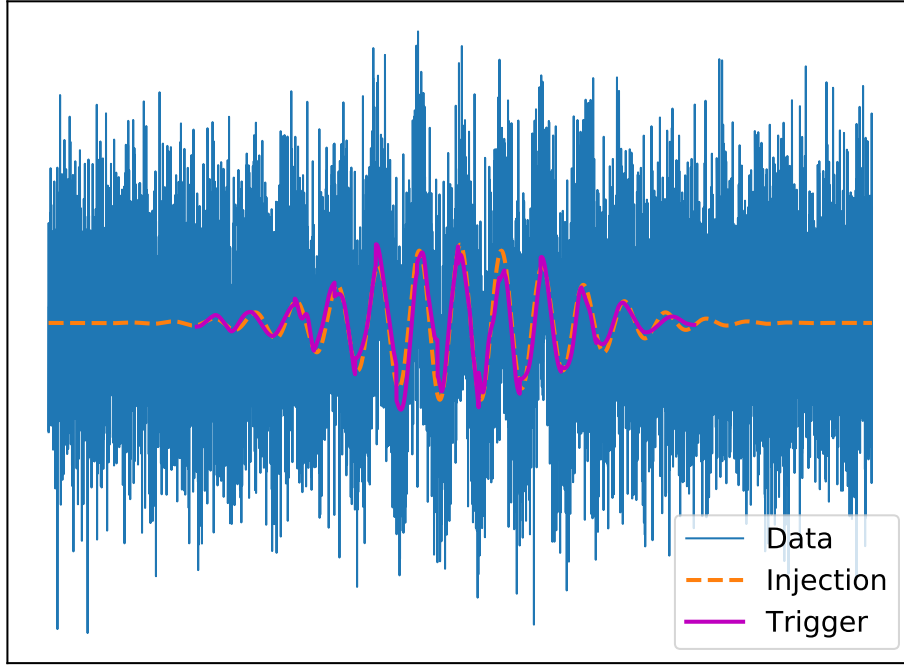


**Figure 6.** Waveform reconstruction of a sine-Gaussian injection (orange, dashed). An event trigger's waveform (purple) can be reconstructed by superposing all excesses that comprise the event trigger. We compute SNR of the event trigger using its reconstructed waveform by applying (6). The thin blue line represents the original data that contains sine-Gaussian waveform with noise. Note that the reconstructed waveform recovers the injected sine-Gaussian waveform with small discrepancy.

$t_e$ , the high frequency  $f_{\text{high}}$  and the low frequency  $f_{\text{low}}$  determine a square section in time-frequency plane, as seen in figure 5. The high and low frequencies are selected as the upper and lower quartiles in the frequency distribution of the corresponding IMF between  $t_s$  and  $t_e$ . Each square in figure 5 represents an excess and the overlapped excesses are clustered into an event trigger. The squares may be stretched to reflect some tolerances in time and/or frequency. If another excess is overlapped one of the excesses in an event trigger, then it should be clustered into the same event trigger. For example, in figure 5, the excesses 5 and 6 are overlapped each other and so they form an event trigger. The excesses 7 and 8 are overlapped with neither of 5 and 6, so they are not clustered in the same event trigger at the moment. After the excess 9 is clustered in the event trigger since it is overlapped with 6, the excess 8 is now overlapped with 9 and is clustered into the event trigger. The excess 7 overlaps with 10 to form the last event triggers in this example. There are four event triggers in figure 5: one with the excess 1, another with 2, 3 and 4, and the others with 5, 6, 8 and 9 and with 7 and 10. The peak time, peak frequency, and peak amplitude for an event trigger are chosen as those for the excess that has the largest peak amplitude among the excesses in the cluster.

### 3.3. Signal-to-Noise Ratio from Waveform Reconstruction

An event trigger consists of one or more excesses and each excess can be restored in the time domain, i.e. the corresponding IMF between  $t_s$  and  $t_e$ . Therefore, by superposing the time-series of the excesses in the cluster, the original waveform of the event can be reconstructed. One can calculate the SNR of the event trigger using this reconstructed waveform as

$$\rho = \frac{1}{\sigma} \left[ \int_{T_s}^{T_e} |X(t)|^2 dt \right]^{1/2}, \quad (6)$$

where  $T_s = \min\{t_s\}$  and  $T_e = \max\{t_e\}$  are the start and end times of the event trigger, respectively, and  $X(t)$  is the reconstructed waveform by superposing the excesses.

The SNR computed from the reconstructed waveform is *little* higher than that computed from (5). However, the accuracy of the SNR recovery depends on how precisely superposed waveform is reconstructed, i.e. how accurate the decomposed IMFs are. To enhance the accuracy of the recovery, one can perform more precise algorithm of finding excesses and clustering but it always produces a trade-off with computation time. Indeed, the overcome of uncertainty between time-frequency resolution might be transferred to the uncertainty between definite algorithm and computation time.

## 4. The performance of the EtaGen: Comparison to Omicron

In this section, the performance of the EtaGen is compared to that of the Omicron based on *Q-transform* which is *currently* the best performing event trigger generator used in the GW data analysis [24].

The performance of the EtaGen may be investigated quantitatively by observing how many artificial transients injected in a background noise can be found. We generated simulated Gaussian noise colored to have the same noise curve as the Advanced LIGO (aLIGO) detectors at design sensitivity. We then injected sine-Gaussians and white noise bursts 30 seconds apart as target signals for recovery. The total number of sine-Gaussian (white noise burst) injections is 3132 (3121). The injections are almost uniformly distributed in both SNR and frequency.

We set the SNR threshold for event triggers (excesses) in the EtaGen to 5.5 (2.75). One can increase the number of excesses by lowering the SNR threshold. However, if we have a excessively large number of excesses by decreasing the threshold to a very small value, the clustering algorithm produces event triggers with unrealistically long duration which are obviously far from the real event triggers. We empirically choose the SNR threshold value of 2.75 for excess to achieve balance between the number of excesses and the duration of *the clustered* event triggers after running many tests.

Consequently, EtaGen finds in total 95.47% of the injections; 99.74% for sine-Gaussian and 91.19% for white noise burst, respectively. As for the timing accuracy, the STD of the timing error of all injections is  $8.32 \times 10^{-3}$  s; sine-Gaussian  $4.49 \times 10^{-3}$  s

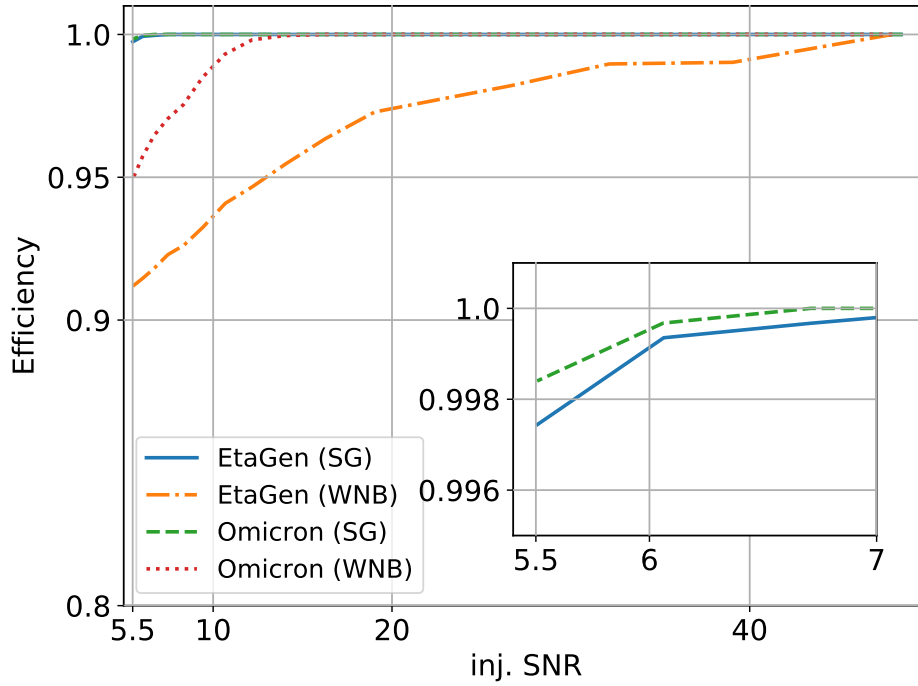


**Figure 7.** The comparison of event trigger generator performance between EtaGen and Omicron for sine-Gaussian (SG) and white noise burst (WNB) injections

and white noise burst  $1.11 \times 10^{-2}$  s. The STD of the frequency error of all injections is 381.07 Hz; sine-Gaussian 223 Hz and white noise burst 497 Hz.

One can compare these results to the performance from Omicron, having efficiency of 99.80 % (sine-Gaussian) and 95.20 % (white noise burst), timing accuracy of  $3.4 \times 10^{-4}$  s (sine-Gaussian) and  $9.8 \times 10^{-3}$  s (white noise burst), and frequency accuracy of 82 Hz (sine-Gaussian) and 152 Hz (white noise burst). We conclude that the efficiency for finding event triggers of EtaGen is comparable with the Omicron. However, the timing and frequency accuracies of triggers are worse than those of Omicron for sine-Gaussian (white noise burst) waveform. The results of the event trigger generator performance tests and comparison to Omicron are seen in figure 7, and detailed results are summarized in table 1.

## 5. Discussion

We have developed EtaGen, a new event trigger generator based on HHT utilizing the adaptive nature of the transform. In order to evaluate its performance, we compare the efficiency and accuracy of EtaGen with those of Omicron by running the event trigger generator on the aLIGO simulated data with two different types of injected signals; sine-Gaussian and white noise burst. As summarized in table 1, the result shows that the efficiency of EtaGen in finding event triggers are comparable to that of Omicron, which is the first step of demonstration as a viable event trigger generator.

**Table 1.** The event trigger generator performance for EtaGen and Omicron with SNR threshold 5.5 is shown. The numbers in the efficiency and timing/frequency accuracies are given by [(number of found injections)/(total number of injections)] $\times 100\%$ ,  $\text{std}[(\text{trigger time})-(\text{injection time})]$ , and  $\text{std}[(\text{trigger frequency})-(\text{injection frequency})]$ , respectively.

Performance tests		EtaGen SNR threshold 5.5	Omicron SNR threshold 5.5
Efficiency	sine-Gaussian	99.74 %	99.8 %
	white noise burst	91.19 %	95.2 %
Timing accuracy	sine-Gaussian	$4.49 \times 10^{-3}$ s	$3.4 \times 10^{-4}$ s
	white noise burst	$1.11 \times 10^{-2}$ s	$9.8 \times 10^{-3}$ s
Frequency accuracy	sine-Gaussian	223 Hz	82 Hz
	white noise burst	497 Hz	152 Hz

The inaccuracy in timing and frequency can arise from errors in weighted SEMD due to parameters chosen such as  $N$ ,  $L$  and the weighting function. Increasing  $N$  and  $L$  might help to obtain more precise IMFs because it corresponds to increasing the ensemble size, although the decomposition process becomes computationally expensive. More sophisticated excess finding procedure using better SNR calculation and an alternative cutoff criterion (see, e.g., [25]) can also improve the accuracy. In fact, we observe improvement in the accuracies and efficiency of recovering triggers by changing SNR calculation from (5) to (6) increases.

As stated at the beginning of this paper, it is anticipated that EtaGen will show better performance in recovering low frequency triggers because of the adaptive nature of the mode decomposition. The time-frequency accuracy trade-off that appears in other event trigger generators utilizing fixed harmonic bases for decomposition such as Fourier transform and wavelet transform is expected to be less severe in EtaGen. This is under investigation and will be reported in a separate article.

## Acknowledgments

The authors would like to thank Jay Tasson for helpful comments and suggestions and Chris Pankow for letting us to use the simulated GW data. EJS is grateful to Hyoungeok Chu for the fruitful contribution to the early stage of this work. YMK was supported by the National Research Foundation of Korea (NRF) grant funded by the Korea government (MSIP) (No. 2016R1A5A1013277). LIGO was constructed by the California Institute of Technology and Massachusetts Institute of Technology with funding from the National Science Foundation and operates under cooperative agreement PHY-0757058. This paper carries LIGO Document Number LIGO-P1800294.

## References

- [1] B. P. Abbott et al. GW150914: Implications for the stochastic gravitational wave background from binary black holes. *Phys. Rev. Lett.*, 116(13):131102, 2016.
- [2] B. P. Abbott et al. GW151226: Observation of Gravitational Waves from a 22-Solar-Mass Binary Black Hole Coalescence. *Phys. Rev. Lett.*, 116(24):241103, 2016.
- [3] Benjamin P. Abbott et al. GW170104: Observation of a 50-Solar-Mass Binary Black Hole Coalescence at Redshift 0.2. *Phys. Rev. Lett.*, 118(22):221101, 2017.
- [4] B. P. Abbott et al. GW170608: Observation of a 19-solar-mass Binary Black Hole Coalescence. *Astrophys. J.*, 851(2):L35, 2017.
- [5] B. P. Abbott et al. GW170814: A Three-Detector Observation of Gravitational Waves from a Binary Black Hole Coalescence. *Phys. Rev. Lett.*, 119(14):141101, 2017.
- [6] Benjamin P. Abbott et al. GW170817: Observation of Gravitational Waves from a Binary Neutron Star Inspiral. *Phys. Rev. Lett.*, 119(16):161101, 2017.
- [7] LK Nuttall, T J Massinger, J Areeda, J Betzwieser, S Dwyer, A Effler, R P Fisher, P Fritschel, J S Kissel, A P Lundgren, D M Macleod, D Martynov, J McIver, A Mullavey, D Sigg, J R Smith, G Vajente, A R Williamson, and C C Wipf. Improving the data quality of advanced ligo based on early engineering run results. *Classical and Quantum Gravity*, 32(24):245005, 2015.
- [8] B. P. Abbott et al. Characterization of transient noise in Advanced LIGO relevant to gravitational wave signal GW150914. *Class. Quant. Grav.*, 33(13):134001, 2016.
- [9] Norden E Huang and Samuel S P Shen. *Hilbert-Huang Transform and Its Applications*. WORLD SCIENTIFIC, 2005.
- [10] Norden E. Huang, Zheng Shen, Steven R. Long, Manli C. Wu, Hsing H. Shih, Quanan Zheng, Nai-Chyuan Yen, Chi Chao Tung, and Henry H. Liu. The empirical mode decomposition and the hilbert spectrum for nonlinear and non-stationary time series analysis. *Proc. R. Soc. Lond. A*, 454(1971):903–995, 1998.
- [11] Norden E. Huang and Zhaohua Wu. A review on hilbert-huang transform: Method and its applications to geophysical studies. *Reviews of Geophysics*, 46(2):RG2006, 2008.
- [12] Jordan B. Camp, John K. Cannizzo, and Kenji Numata. Application of the Hilbert-Huang Transform to the Search for Gravitational Waves. *Phys. Rev.*, D75:061101, 2007.
- [13] Alexander Stroeer, John K. Cannizzo, Jordan B. Camp, and Nicolas Gagarin. Methods for detection and characterization of signals in noisy data with the Hilbert-Huang transform. *Phys. Rev.*, D79:124022, 2009.
- [14] Alexander Stroeer and Jordan Camp. Ninja data analysis with a detection pipeline based on the Hilbert-Huang Transform. *Class. Quant. Grav.*, 26:114012, 2009.
- [15] Masato Kaneyama, Ken-ichi Oohara, Hirotaka Takahashi, Yuichiro Sekiguchi, Hideyuki Tagoshi, and Masaru Shibata. Analysis of gravitational waves from binary neutron star merger by Hilbert-Huang transform. *Phys. Rev.*, D93(12):123010, 2016.
- [16] Kazuki Sakai, Ken-Ichi Oohara, Hiroyuki Nakano, Masato Kaneyama, and Hirotaka Takahashi. Estimation of starting times of quasi-normal modes in ringdown gravitational waves with the Hilbert-Huang transform. *Phys. Rev.*, D96(4):044047, 2017.
- [17] Guillermo Valdes, Brian O'Reilly, and Mario Diaz. A HilbertHuang transform method for scattering identification in LIGO. *Class. Quant. Grav.*, 34(23):235009, 2017.
- [18] P. Flandrin, G. Rilling, and P. Goncalves. Empirical mode decomposition as a filter bank. *IEEE Signal Processing Letters*, 11(2):112–114, Feb 2004.
- [19] Norden E Huang, Man-Li C Wu, Steven R Long, Samuel S.P Shen, Wendong Qu, Per Gloersen, and Kuang L Fan. A confidence limit for the empirical mode decomposition and hilbert spectral analysis. *Proc. R. Soc. Lond. A*, 459(2037):2317–2345, 2003.
- [20] Gang Wang, Xian-Yao Chen, Fang-Li Qiao, Zhaohua Wu, and Norden E. Huang. On intrinsic mode function. *Adv. Adapt. Data Anal.*, 02(03):277–293, 2010.
- [21] Zhaohua Wu and Norden E. Huang. Ensemble empirical mode decomposition: A noise-assisted

- data analysis method. *Adv. Adapt. Data Anal.*, 01(01):1–41, 2009.
- [22] R. Faltermeier, A. Zeiler, I. R. Keck, A. M. Tom, A. Brawanski, and E. W. Lang. Sliding empirical mode decomposition. In *The 2010 International Joint Conference on Neural Networks (IJCNN)*, pages 1–8, July 2010.
- [23] R. Faltermeier, A. Zeiler, A. M. Tomé, A. Brawanski, and E. W. Lang. Weighted sliding empirical mode decomposition. *Adv. Adapt. Data Anal.*, 03(04):509–526, 2011.
- [24] Jessica L. McIver. *The impact of terrestrial noise on the detectability and reconstruction of gravitational wave signals from core-collapse supernovae*. PhD thesis, Massachusetts U., Amherst, 2015.
- [25] Peter J. Rousseeuw and Christophe Croux. Alternatives to the median absolute deviation. *Journal of the American Statistical Association*, 88(424), 1993.